# Homogeneous Catalytic Processes Monitored by Combined *in Situ* ATR-IR, UV−Vis, and Raman Spectroscopy

Kathleen Grabow and Ursula Bentrup*

Leibniz-Institut für Katalyse e.V. an der Universität Rostock (LIKAT), Albert-Einstein-Str. 29a, 18059 Rostock, Germany

ABSTRACT: The benefit of coupling *in situ* spectroscopic methods (attenuated total reflectance-infrared spectroscopy (ATR-IR), Raman, and UV−vis) for the real-time monitoring of homogeneously catalyzed reactions is exemplarily demonstrated on selected examples of use. In this context, the different mode of catalyst action in reduction reactions of imides and amides with phenylsilanes will be discussed. In the iron-catalyzed decomposition of formic acid, different intermediate iron complexes were identified and the inhibiting effect of chloride onto active iron complex formation could be elucidated. Furthermore, it could be shown that in a Lewis acid catalyzed cyclocondensation reaction, the reactant activation proceeds differently with $AlCl_3$ and $TiCl_4$. For the described *in situ* spectroscopic studies, a versatile setup was used which allows the simultaneous registration of ATR-IR, UV−vis, and Raman spectra in small volumes of solution at different reaction-determined conditions using fiber-optic probes for the each spectroscopy.
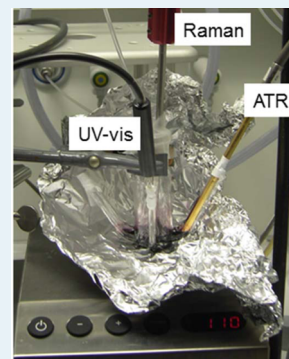
KEYWORDS: homogeneous catalysis, in situ spectroscopy, reduction, phenyl silane, formic acid, iron, cyclization, Lewis acid

1. INTRODUCTION

For elucidating the mechanism of catalytic reactions and the identification of catalytic active species, sophisticated *in situ* characterization methods and combinations of them are substantial to get insight into catalyst acting under real reaction conditions. Furthermore, *in situ* spectroscopy is the only approach to derive reliable information on the role of intermediates in chemical reactions as well as on structure−reactivity relationships in catalysis.[1−4] In heterogeneous catalysis, the application of a variety of *in situ* methods has gained a lively development during the last 2 decades. However, also in homogeneous catalysis as well as in catalytic multiphase systems, *in situ* characterization methods are increasingly used.[5−8] Besides X-ray absorption spectroscopic methods like X-ray absorption near edge structure (XANES) and extended X-ray absorption fine structure (EXAFS), which should not be further discussed here, vibrational and magnetic resonance spectroscopic methods like attenuated total reflectance-infrared spectroscopy (ATR-IR), UV−vis, Raman, electron paramagnetic resonance (EPR), and NMR were applied for the study of several types of catalytic reactions proceeding in the liquid phase.[9−23]

Referring to magnetic resonance methods (NMR and EPR), particularly NMR is widely used for reaction monitoring, also under higher pressures.[5,8,18] However, NMR is not applicable to all nuclei, and quenching problems may occur in the presence of paramagnetic species. Otherwise, EPR spectroscopy can only detect species with unpaired electrons. This limits the application potential for this method, and additional complementary methods like UV−vis spectroscopy are necessary to characterize diamagnetic species too.

Raman and IR spectroscopy provide complementary information. Because of different requirements concerning the excitation of respective vibrations (IR spectroscopy requires groups with a permanent dipole moment, Raman spectroscopy needs groups which have polarizable bonds), certain vibrations of functional groups are active or inactive in the infrared or Raman spectra, respectively. While IR spectroscopy enables the identification of characteristic functional groups by inspecting the range between 4000 and 700 cm^{-1}, bands resulting from metal−nonmetal vibrations appearing in the low frequency range (1000−200 cm^{-1}) can be observed well with Raman spectroscopy. Consequently, the combination of both methods provides comprehensive information about the vibrational state of molecules, in particular when metal complexes are participating in catalytic reactions.

UV−vis spectroscopy gives less distinct information about the molecular structure because of the appearance of rather broad bands. The bands observable in the UV−vis spectra of organic molecules are prominent for chromophores or indicate charge transfer between metal and ligands as well as changes of oxidation state in metal complexes. For this reason, UV−vis spectroscopy is a powerful tool to study changes in complex molecules influenced by distinct interactions with ligands and solvent molecules.

To get mechanistic insights into the relevant reaction and to gain knowledge concerning the specific catalyst mode of action as well as the importance of the solvent interaction, the coupling of spectroscopic methods provides a more complete picture due to the increased amount of incoming information. The simultaneous usage of different methods in the same catalytic reactor also offers maximum reliability of the obtained

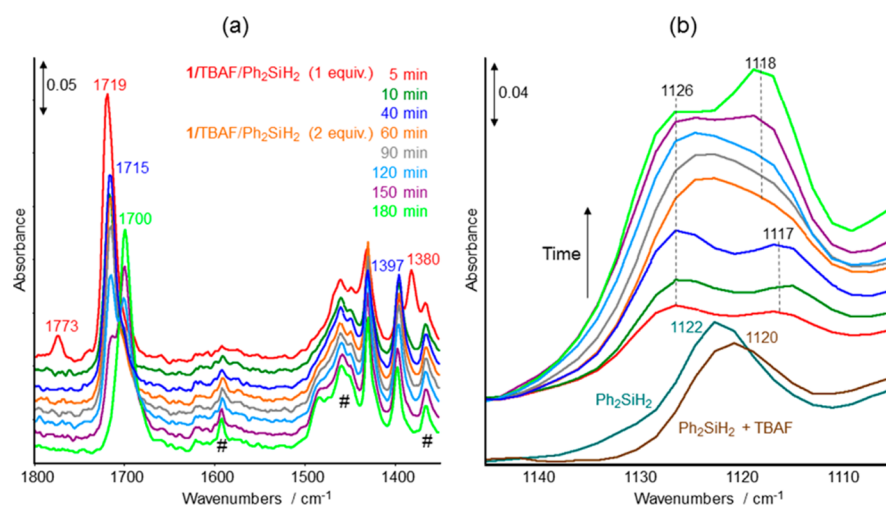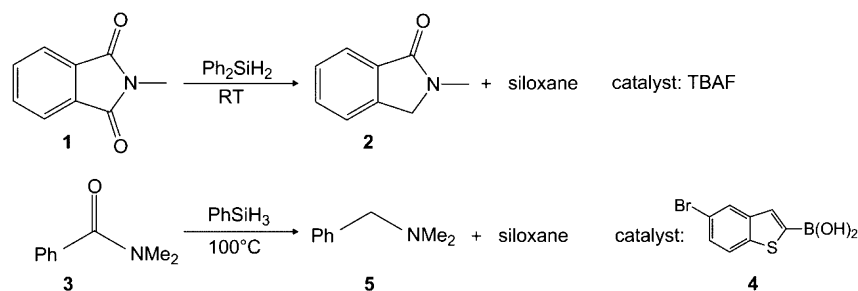**Scheme 1. Hydrosilylation Reactions of Imides and Amides**

Figure 1. *In situ* ATR-IR spectra recorded during reaction of **1** (644 mg) and Ph_2SiH_2 (2.234 mL) in THF (14 mL) with TBAF (0.2 mL) as catalyst at room temperature: spectral ranges 1800−1350 cm^{-1} (a) and 1145−1105 cm^{-1} (b). THF bands are assigned by hashmarks. Reproduced with permission from ref 33. Copyright 2011 John Wiley & Sons, Inc.

results. In recent decades several studies were published in literature showing the application of different spectroscopic methods or combinations of them for the monitoring of homogeneously and heterogeneously catalyzed reactions in the liquid phase, even under unusual conditions of high pressures or low temperatures.[6,24−34]

In the following, the benefit of method coupling will be exemplarily demonstrated on selected examples of use, whereat the presented studies are focused on the application of *in situ* ATR-IR, Raman, and UV−vis spectroscopy. It will be shown how *in situ* spectroscopies can help to answer questions concerning mechanistic aspects arising from the specific type of catalytic reaction. In this context, the catalyst action in reduction reactions of imides and amides with phenylsilanes will be discussed, the detection of active and inactive catalyst species in the Fe-catalyzed decomposition of formic acid, and the specific catalyst−reactant interaction in Lewis acid catalyzed cyclocondensation reactions. For this purpose a versatile setup was used,[32−34] which allows the simultaneous registration of ATR-IR, UV−vis, and Raman spectra in small volumes of solution at different reaction-determined conditions and temperatures using fiber-optic probes for each spectroscopy.

2. SELECTED CATALYTIC REDUCTIONS WITH PHENYLSILANES

Das et al.[33] described the fluoride-catalyzed monoreduction of phthalimides and Li et al.[34] the boronic-acid catalyzed selective reduction of amides to amines using phenylsilanes as the hydrogenating agent. These two types of reaction were

exemplarily displayed in Scheme 1. In both cases the question has to be answered in which way the catalyst acts: (i) activating the educts or (ii) activating the respective phenylsilanes. For mechanistic studies, the reaction of *N*-methylphthalimide **1** to *N*-methylisoindolinone **2** using tetra-*n*-butylammonium fluoride (TBAF) as the catalyst and the boronic acid catalyzed reaction of *N,N*-dimethylbenzamide **3** to *N,N*-dimethylbenzamine **4** were investigated (Scheme 1).

Combined *in situ* ATR-IR and UV−vis spectroscopic investigations showed that for the first reaction no interaction between the imide **1** and the catalyst TBAF takes place.[33] In the ATR-IR spectra (Figure 1a), characteristic bands of **1** at 1773, 1719, and 1380 cm^{-1} can be seen besides the bands of the solvent (THF), which are assigned to ν_sC=O, ν_{as}C=O, and δ_sCH$_3$, respectively. These band positions were not affected by addition of TBAF. Whereas Ph_2SiH_2 dissolved in THF gives only one νSi−Ph band at 1122 cm^{-1}, the position of which shifts to 1120 cm^{-1} by adding TBAF, and a further splitting of this band is observed in the presence of **1** (Figure 1b). This band shift clearly indicate an interaction of TBAF with Ph_2SiH_2 and additionally, in the presence of **1**, with the imide too. After 10 min reaction time, the ν_{as}C=O band showed a slight shift from 1719 to 1715 cm^{-1} while the ν_sC=O band at 1773 cm^{-1} and the δ_sCH$_3$ band at 1380 cm^{-1} completely disappeared. In turn, the δ_sCH$_3$ band at 1397 cm^{-1} became dominant.

The UV−vis spectrum of the reactant **1** in THF did not change after addition of TBAF and is characterized by bands at 265, 302, and 324 nm resulting from conjugated interaction of the two carbonyl chromophores with the electron pair of the

nitrogen (Figure 2). While the addition of one equivalent Ph_2SiH_2 caused no significant changes within the first 5 min of
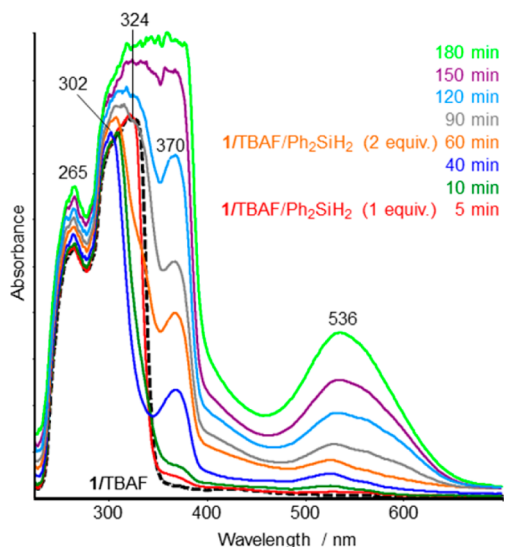

Figure 2. *In situ* UV−vis spectra recorded during reaction of **1** and Ph_2SiH_2 with TBAF as catalyst at room temperature. The component concentrations are the same as denoted in Figure 1. Reproduced with permission from ref 33. Copyright 2011 John Wiley & Sons, Inc.

reaction, the band at 324 nm vanished after 10 min indicating the beginning reduction of one carbonyl group. Simultaneously, a new band at 370 nm started to appear resulting from the product **2** as confirmed by a separate measurement of its UV−vis spectrum in THF.

To reach progressive product formation, the addition of the second equivalent Ph_2SiH_2 is indispensable. During the course of reaction, the formation of **2** is observed by rising of the respective bands in the ATR-IR (1700 cm^{-1}) as well as in the UV−vis (370 nm) spectra. The intensities of the $\nu C{=}O$ band of the product **2** at 1700 cm^{-1} and the $\nu Si-Ph$ band at 1126/1117 cm^{-1} increase simultaneously (Figure 1). The latter effect is obviously caused by the formation of $Ph_2HSi-O-SiHPh_2$ because $Si-O-Si$ as well as $Si-Ph$ vibrations are observed in this range. The increasing product formation is also seen by the rising intensity of the band at 370 nm in the UV−vis spectra (Figure 2). The additional band, growing at 536 nm, points to the formation of molecules with highly conjugated chromophors which are formed in small amounts as side products.

On the basis of the findings of the *in situ* measurements and in accordance with former assumptions concerning the activation of Si−H bonds,[35] it was assumed from the observed band shift of $\nu Si-Ph$ that in the first step of the catalytic cycle fluoride is coordinated to the silicon atom of Ph_2SiH_2 forming a reactive penta-coordinated silicon species. This species immediately attacks the carbonyl group of **1** giving a hexa-coordinated silicon species within which the hydride transfer can take place (Scheme 2). Consumption of the respective bands in the ATR-IR as well as in the UV−vis spectra confirmed this assumption. As a consequence, besides the product **2** $Ph_2HSi-O-SiHPh_2$ is formed indicated by the appearance of two bands at 1126 cm^{-1} ($\nu Si-Ph$) and 1117 cm^{-1} ($\nu Si-O-Si$) whereat the latter increases significantly with reaction progress (Figure 1b). The phenylsiloxane formation seems to be a driving force for this reaction. Furthermore, it is

Scheme 2. Proposed Reaction Mechanism for the Monoreduction of Phthalimide 1
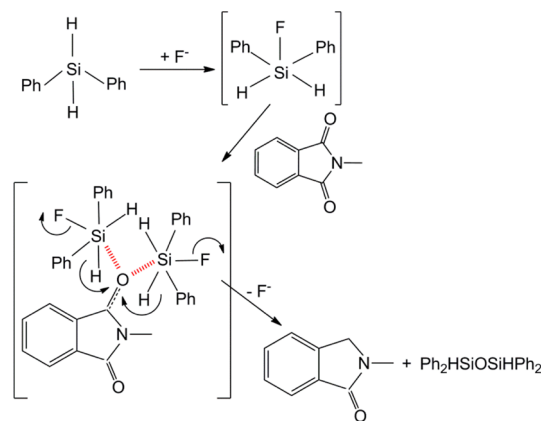
obvious that two equivalents of Ph_2SiH_2 are required to get an effective and selective reduction of the imide.

For the boronic-acid catalyzed selective reduction of amides to amines using $PhSiH_3$ as the hydrogenating agent, it could be shown that the catalyst acts in a different manner.[34] From the simultaneous *in situ* ATR-IR and UV−vis spectroscopic measurements, the reaction progress could be observed very well (Figure 3).

The intensities of the carbonyl band and the silane band decrease with time (because of its high intensity the latter cannot be seen in Figure 3b), while new bands appear at 1147 and 1133 cm^{-1} (Figure 3a,b). Simultaneously, the absorption edge in the UV−vis spectra (Figure 3c) is shifted to higher wavelengths and a new band grows up at 360 nm. Because the bands at 1147 and 1133 cm^{-1} stem from $\nu Si-O-Si$ modes of different siloxanes, the new band in the UV−vis spectrum at 360 nm should be a result of additional coordination effects of siloxane moieties. Both, the decreasing $\nu Si-H$ band intensity and the simultaneous increasing of the UV−vis band intensity at 360 nm correlate well and demonstrate the reaction progress as indicated by siloxane formation. Although this *in situ* experiment allows the real-time monitoring of the reduction process, unfortunately the direct mode of action of the catalyst could not be observed. Hence, different experiments were additionally performed to study the interaction of the catalyst **4** with both, the $PhSiH_3$ and the amide **3**, separately.

The spectrum of catalyst **4** dissolved in toluene is characterized by bands at 1353 and 1170 cm^{-1} (Figure 4) which are related to the typical $\nu B-O(H)$ and $\nu B-C$ modes of boronic acids.[36] In mixtures of **4** and $PhSiH_3$, these bands are also visible even after heating the mixture at 90 °C for 30 min, and the positions of the typical silane bands at 1429 and 1117 cm^{-1} are not affected too. However, if the amide **3** is added to this mixture, the original $\nu B-O$ band vanishes while the $\nu B-C$ mode does not change. Similarly, the spectrum of a mixture of catalyst **4** and amide **3** in toluene without the silane shows this $\nu B-C$ band but not the $\nu B-O$ mode (Figure 4). Moreover, a shift of the $\nu C{=}O$ band from 1643 to 1646 cm^{-1} is observed which is less pronounced as in the *in situ* experiment because of the lower temperature.

These findings clearly suggest an interaction of the boronic acid with the amide via hydrogen bonding between OH groups of the boronic acid and the carbonyl group of the amide. Such hydrogen bond formation between boronic acids and the respective carbonyl groups of carboxylic acids and amides have
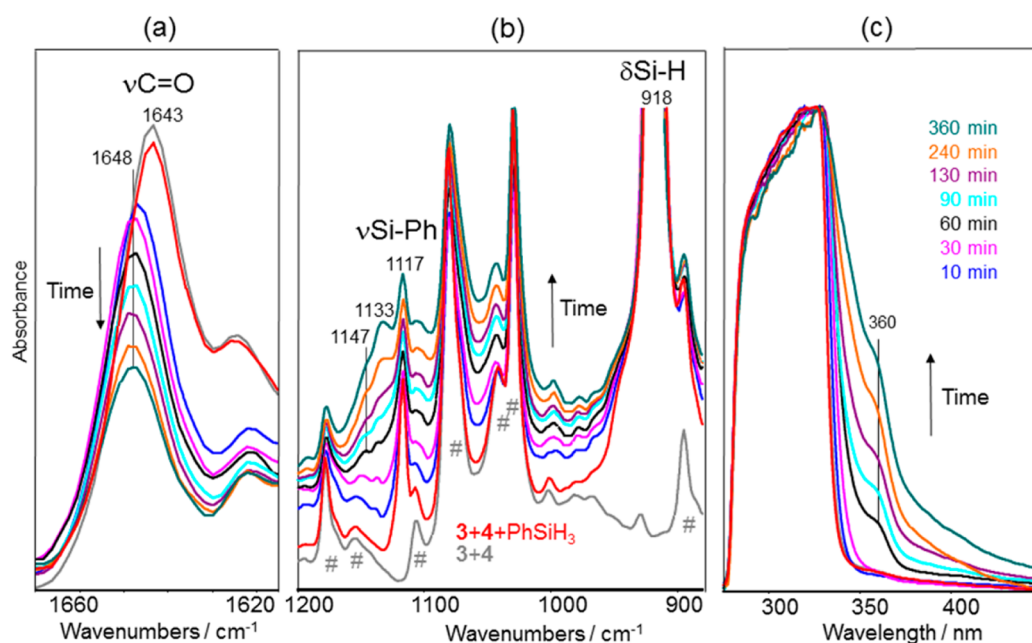
Figure 3. *In situ* ATR-IR spectra (a, b) and *in situ* UV−vis (c) spectra recorded during reaction of **3** (223.5 mg) and PhSiH$_3$ (0.45 mL) in toluene (6 mL) with boronic acid **4** (96 mg) as catalyst at 100 °C (toluene bands assigned by hashmarks). Adapted with permission from ref 34. Copyright 2013 John Wiley & Sons, Inc.
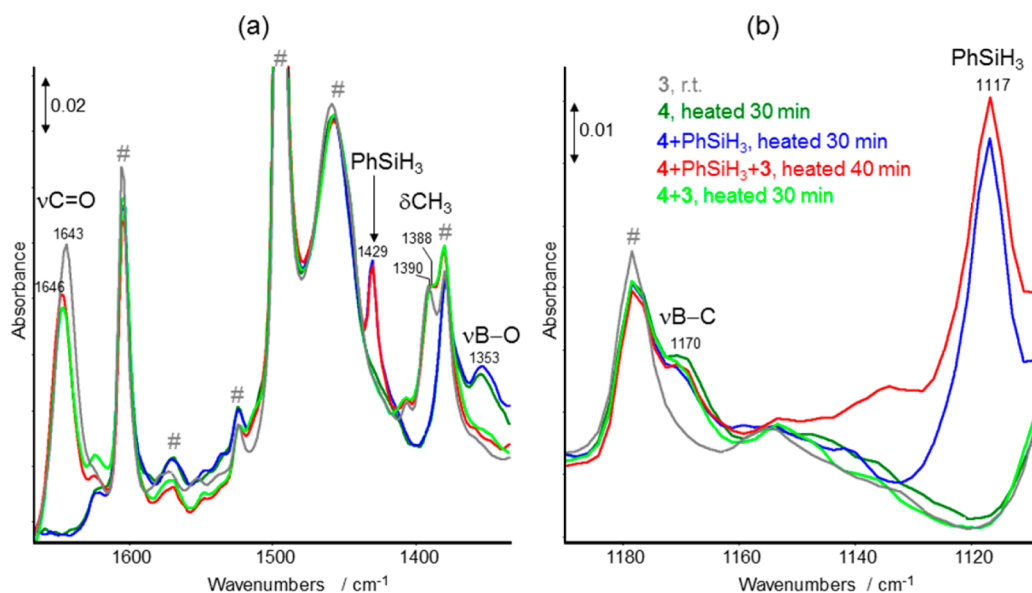

Figure 4. ATR-IR spectra of **4** and mixtures of **4** with PhSiH$_3$ and **3**, respectively, obtained after heating at 90 °C in toluene. The spectrum of **3** in toluene at room temperature is shown for comparison (toluene bands assigned by hashmarks): spectral ranges 1700−1300 cm^{-1} (a) and 1190−1110 cm^{-1} (b). The component concentrations were the same as used in the *in situ* experiment (cf. Figure 3). Reproduced with permission from ref 34. Copyright 2013 John Wiley & Sons, Inc.

also been described in the literature.[37,38] This assumption is additionally confirmed by results from the simultaneously measured UV−vis spectra. While **4** as well as the mixture of **4** + PhSiH$_3$ in toluene at 90 °C give identical spectra, the addition of **3** to the latter mixture causes a significant blue-shift which indicates an interaction of **4** and **3**.

On the basis of the spectroscopic findings, a possible activation mode for the boronic acid-catalyzed amide reduction with PhSiH$_3$ is presented in Scheme 3. The main point is the activation of the amide carbonyl group via hydrogen bonding with the OH groups of the boronic acid. This enables the direct attack of the silane and subsequent hydrogen transfer leading to the formation of amine **5** and siloxane. Taking into account the possible structure of the complex formed by hydrogen bonding between **3** and **4**, the simultaneous attack of three silane molecules is imaginable (cf. Scheme 3), which would be lead to higher siloxanes.

A summary can be stated that *in situ* spectroscopic investigations could help to elucidate the different mode of catalyst action as demonstrated on two exemplary reactions in which one carbonyl group of amides or imides is reduced by phenylsilanes. Depending on the type of catalyst used, either

Scheme 3. Proposed Reaction Mechanism for the Boronic-Acid Catalyzed Reduction of Amide 3 to the Respective Amine 5
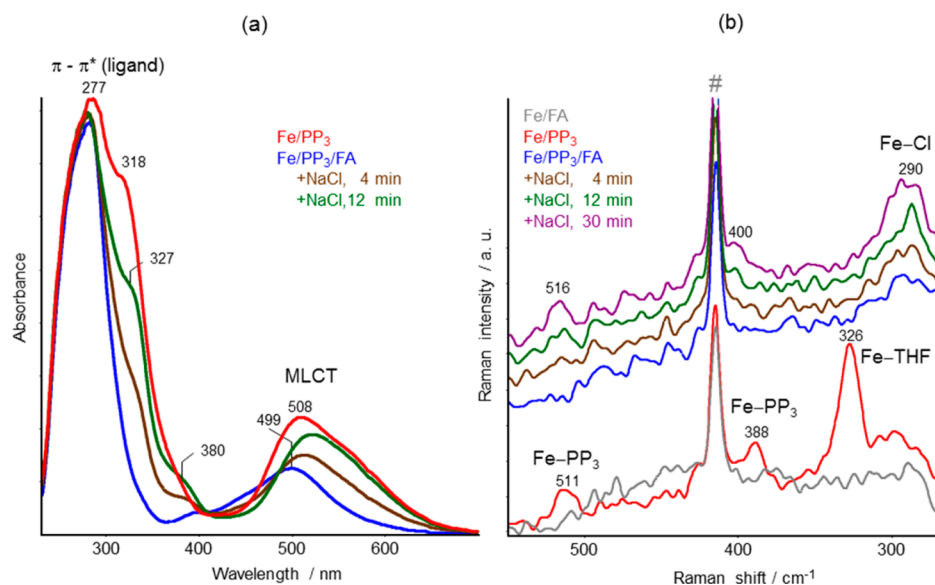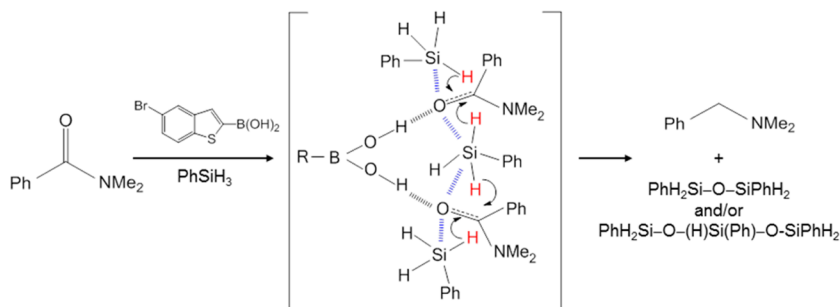

Figure 5. *In situ* UV−vis (a) and Raman spectra (b) obtained from Fe/PP$_3$ in THF, after addition of FA, and subsequent admixture of NaCl after 4, 12, and 30 min: (a) 1.78 mg of Fe, 7.62 mg of PP$_3$, 5 mL of THF, 2 mL of FA, 4.54 mg of NaCl; (b) 105 mg of Fe, 303.5 mg of PP$_3$, 5 mL of THF, 3 mL of FA, 18.2 mg of NaCl. The band from the Raman probe itself is marked by a hashmark.

the silane or the carbonyl group of the amide/imide is activated. In both reactions, the formation of phenylsiloxanes seems to be a driving force.

3. IRON CATALYZED CATALYTIC DECOMPOSITION OF FORMIC ACID

Formic acid (FA) has attracted attention as a suitable liquid source for hydrogen and as potential hydrogen storage material.[39] Furthermore, by using CO$_2$ as a C1-source, a sustainable and reversible energy storage cycle is imaginable.[40] Recently, a well-defined iron catalyst system was described enabling the decomposition of FA to H$_2$ and CO$_2$ in acidic media at ambient conditions with catalyst activities comparable to the best known noble metal catalysts.[41] The benefit of this iron-based catalyst system, formed *in situ* from Fe(BF$_4$)$_2$·6H$_2$O (Fe) and the tetradentate ligand tris[(2-diphenylphosphino)-ethyl]phosphine (P(CH$_2$CH$_2$PPh$_2$)$_3$, PP$_3$), is that no additional additives or sophisticated reaction setups are required. Presynthesized catalysts, for example, [FeH(PP$_3$)]BF$_4$, were also shown to be active, while [FeCl(PP$_3$)]BF$_4$ exhibited in principle no activity. Furthermore, it was found that the *in situ* generated catalyst system Fe/PP$_3$ is sensitive toward traces of chloride leading to a drastic drop in activity depending on chloride concentration.[42] Hence, the question arose which intermediate complexes were formed by interaction of the iron

catalyst complex with FA and in which way chloride admixture affects this complex formation. Therefore, a comprehensive *in situ* spectroscopic study comprising simultaneous Raman, UV−vis, and ATR-IR spectroscopy was carried out to get deeper insight into these complex formation processes.

While UV−vis spectra could nicely be measured using the same concentrations as applied in the catalytic experiments,[42] it was not possible to study structural changes of the catalytic active species by Raman and ATR-IR spectroscopy in such solutions with comparable low Fe catalyst precursor concentrations. For this reason, simultaneous *in situ* Raman/UV−vis/ATR-IR spectroscopic investigations were carried out using higher Fe concentrations. As expected, in this case the bands in the UV−vis spectra become very broad without any structuring; however, the observed effects were the same which was checked by analysis of the absorbance at 665 nm (high Fe concentration) and 325 nm (low Fe concentration) during different steps of reaction. In both cases the same trends were observed indicating a comparable reaction behavior.

The *in situ* UV−vis and Raman spectra obtained during the reaction of Fe/PP$_3$ in THF with FA and NaCl are displayed in Figure 5. The UV−vis spectrum of Fe/PP$_3$/THF (Figure 5a) shows two characteristic bands at 277 and 508 nm resulting from $\pi \rightarrow \pi^*$ and MLCT transitions, respectively. For explaining the nature of the observed shoulder at 318 nm, some reference spectra of the single components were
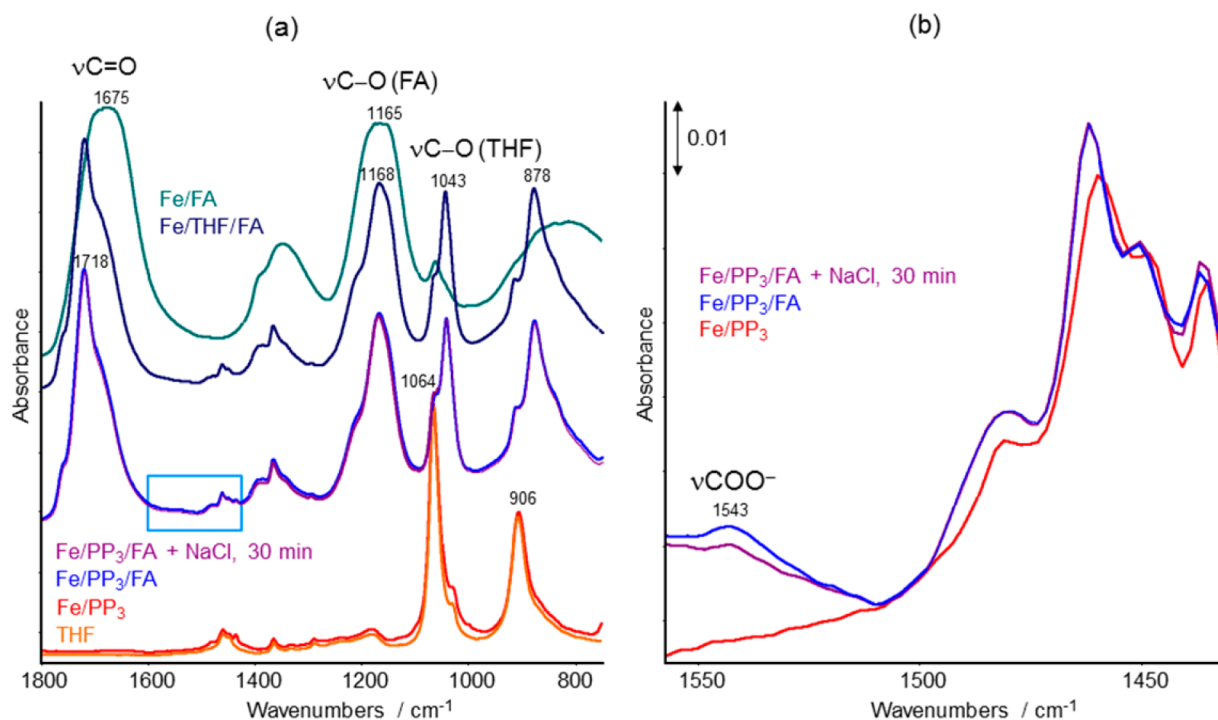
Figure 6. *In situ* ATR-IR spectra obtained from Fe/PP$_3$ in THF, after addition of FA, and subsequent admixture of NaCl after 30 min in the spectral range 1800−775 cm^{-1} (a) and 1555−1435 cm^{-1} (b). The spectra of THF, Fe/FA, and Fe/THF/FA are included for comparison. The component concentrations are the same as denoted in Figure 5b.

recorded. Thus, the spectrum of PP$_3$/THF showed only one band at 277 nm, and the spectrum of Fe/THF a broad low intensity band between 230 and 350 nm. Therefore, it was reasoned that the band at 318 nm in the spectrum of Fe/PP$_3$/THF is caused by an interaction between the Fe/PP$_3$ complex and THF as an additional ligand. This band immediately vanishes when FA is added to the Fe/PP$_3$/THF solution, and the MLCT band at 508 nm loses intensity and shifts to 499 nm. This finding reveals the coordination of FA on the *in situ* generated Fe/PP$_3$ catalyst system by replacing previously coordinated THF. After addition of NaCl, new bands at 327 and 380 nm appear with increasing intensity with dependence on time. Simultaneously, the band at 499 nm shifts continuously to higher wavelengths while their intensity increases too. Both observations indicate a participation of chloride in complex formation. This conclusion was confirmed by measuring the UV−vis spectrum of the separately synthesized compound [FeCl(PP$_3$)]BF$_4$ in THF which shows a similar spectrum as measured in the *in situ* experiment after 12 min.

The inspection of the low wavenumber range of the Raman spectra (Figure 5b) enables some more information concerning the occurrence of specific features characterizing Fe−ligand and Fe−Cl vibrations. Comparing the spectra of Fe/PP$_3$ and Fe/FA, it is evident that the bands at 511, 388, and 326 cm^{-1} appear only in the presence of PP$_3$. While the first two bands result from Fe−PP$_3$ modes in the complex, the latter is related to a Fe−O mode from coordinated THF because in metal aqua complexes metal oxygen modes were observed between 300 and 400 cm^{-1}.[43,44] After addition of FA, the bands at 511 and 388 cm^{-1} vanish first, caused by the diluting effect of the FA admixture but reappear after addition of NaCl. In contrast, the intense band at 326 cm^{-1} does not reappear during the experiment because the former coordinated THF is completely

replaced by coordinatively bonded FA (*vide infra*). This conclusion is in accordance with the UV−vis spectroscopic results revealing changes of the coordination sphere (vanishing of the band at 318 nm) by addition of FA. After subsequent addition of chloride, a new band is observable at 290 cm^{-1}, the intensity of which increases with time (Figure 5b). This band can be assigned to a Fe−Cl vibration[45,46] and reveals the additional coordination of chloride to the Fe/PP$_3$ complex which is in accordance with the findings of the UV−vis spectroscopic investigations too.

Looking at the *in situ* ATR-IR spectra (Figure 6a) gives additional information concerning the coordination of FA. For clarity, the spectral range between 1555 and 1435 cm^{-1} is heightened and displayed in Figure 6b. After addition of FA to the Fe/PP$_3$ solution, the typical νC=O and νC−O bands from FA at 1718 and 1168 cm^{-1} can be seen (Figure 6a). Furthermore, a band at 1543 cm^{-1} appears (Figure 6b) which was not observed in FA/THF and Fe/FA/THF solutions, merely in the presence of PP$_3$. That means, this band is only observable when the Fe-PP$_3$ complex was already formed. The position of this band indicates chelating bidentate formate species formed by the coordination of FA on the Fe-PP$_3$ complex.[47,48] In parallel, the THF bands at 1064 cm^{-1} (νC−O) and 906 cm^{-1} (ring mode) shift to lower wavenumbers caused by the additional interaction of FA with the solvent, in particular via the released protons. After addition of NaCl, the intensity of the formate band decreases (Figure 6b) because chloride is preferred coordinated now which was also confirmed by UV−vis and Raman spectroscopy (*vide supra*).

The coordination of FA on the *in situ* generated Fe-PP$_3$ complex as chelating bidentate formate species was also observed by separately performed FTIR measurements in transmission mode and simultaneous gas (H$_2$ + CO$_2$) analytics.[42] During this *operando* FTIR experiment, it was

found that the evolution of CO_2 and H_2 goes along with formation of the Fe-PP_3-bidentate formate complex. Admixture of NaCl leads to a distinct drop of catalytic activity depending on the NaCl concentration accompanied by vanishing of the formate band at 1543 cm^{-1}.

Taking all spectroscopic findings into account, different iron complex species could be identified which are shown in Scheme 4. From UV–vis and Raman spectroscopic results, it can be

Scheme 4. Possible Iron Complexes Generated in the System Fe(BF_4)$_2$·6H_2O (Fe)/PP_3/FA/NaCl with THF As Solvent
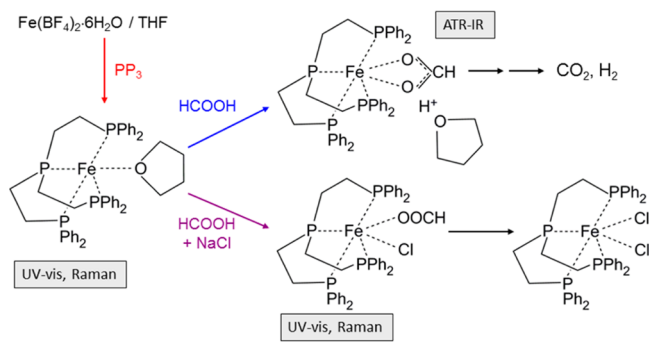
concluded that the Fe-PP_3 complex is formed in the first step while possibly one THF molecule acts as additional ligand to stabilize this complex. The THF ligand is rapidly displaced by FA, and the latter is coordinated as chelating bidentate formate which was proved by FTIR spectroscopy. The solvent THF can act as a stabilizing agent for the protons via hydrogen bonding.

In the presence of NaCl, the coordination of FA as bidentate formate is hindered because chloride is preferentially coordinated as proved by UV–vis and Raman spectroscopy. In the first step the coordination of FA as monodentate formate is imaginable, but finally a complete displacement by chloride ligands has to be assumed. According to the *operando* FTIR experiments, the Fe-PP_3-bidentate formate complex is the catalytically active complex which is obviously indispensable for the evolution of CO_2 and H_2.

This comprehensive *in situ* spectroscopic study nicely demonstrates the benefit of method coupling. Putting together the specific information provided by each method, it was possible to identify different intermediate iron complexes being active or inactive in the catalytic decomposition of FA.

4. LEWIS ACID CATALYZED CYCLOCONDENSATION REACTIONS

Knöpke et al.[32] reported on the utilization of *in situ* spectroscopy to explain the Lewis acid directing effect on the reaction pathway in formal [3 + 3] cyclocondensation reactions. By means of different *ex situ* and *in situ* spectroscopic methods, the mode of action of the Lewis acids $TiCl_4$ and TMSOTf utilized in the [3 + 3] cyclization reaction of a ketenacetales 6 with a diene 7 (Scheme 5) could be elucidated.

The formation of different products dependent on the type of Lewis acid used was explained by two completely different reaction pathways which are mainly directed by the specific interaction of the Lewis acids with the ketenacetale 6.[32] Results of ATR-IR and UV–vis spectroscopic studies revealed that TMSOTf interacts with only one site of the ketenacetale forming an ionic species. In contrast, $TiCl_4$ forms a dichloro bis-chelate complex in which vibrations of the Ti–O and Ti–Cl

Scheme 5. Lewis Acid Catalyzed Cyclization Reaction of Ketenacetale 6 with Diene 7 Giving Salicylate 8
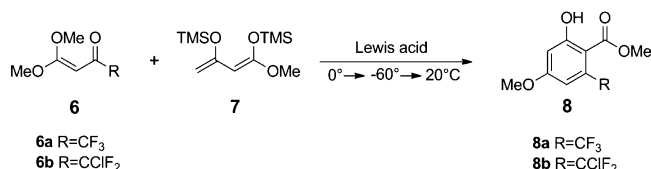
bonds were clearly identified by Raman spectroscopy. The spectroscopic findings were also confirmed by X-ray crystal structure analysis.

In a further work,[49] $AlCl_3$ was used as a Lewis acid and simultaneous *in situ* ATR-IR/UV–vis spectroscopy was carried out for mechanistic studies. Although the same product 8 was obtained with comparable yields, it was shown that the activation of the ketenacetale 6 with $AlCl_3$ proceeds in a different manner as observed for $TiCl_4$. In the following, this aspect will be discussed in more detail.

The *in situ* ATR-IR spectra recorded during the reaction of 6a with 7 in the presence of $AlCl_3$ are displayed in Figure 7.
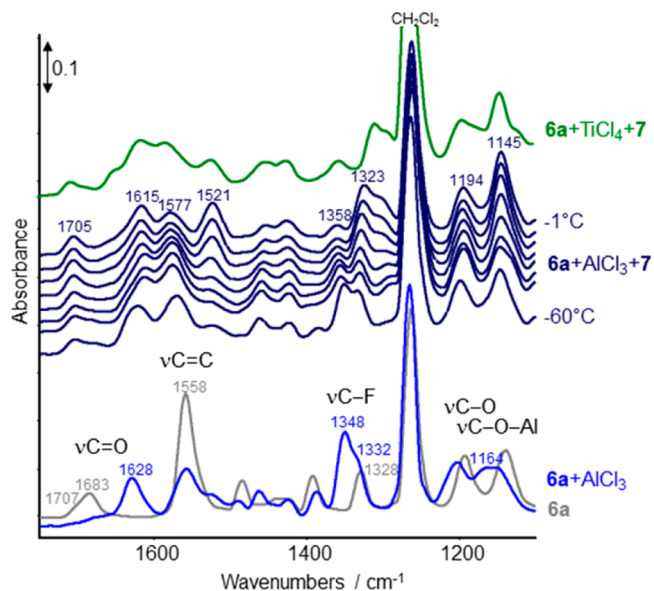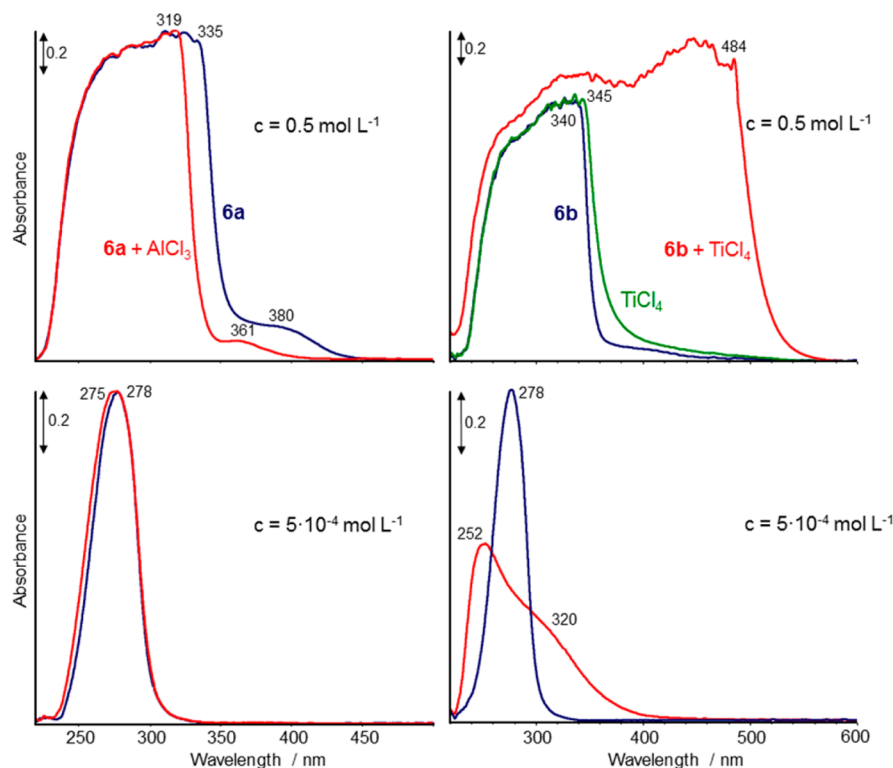
Figure 7. *In situ* ATR-IR spectra recorded during the $AlCl_3$-mediated reaction in CH_2Cl_2 (8 mL): 6a (736 mg, 4 mmol) at 20 °C without $AlCl_3$, 6a + $AlCl_3$ at −60 °C in 1:1-mixture (molar ratio), 6a + $AlCl_3$ + 7 as 1:1:2-mixture (molar ratio) at −60, −50, −40, −30, −20, −10, −5, and −1 °C. The spectrum of 6a + $TiCl_4$ + 7 at −1 °C is shown for comparison. Adapted with permission from ref 32. Copyright 2011 John Wiley & Sons, Inc. Adapted with permission from ref 49. Copyright 2013 Elsevier.

After adding $AlCl_3$ to 6a at 0 °C and cooling to −60 °C, the νC═O band of 6a is shifted to lower wavenumbers and appears at 1628 cm^{-1} with increased intensity indicating an interaction of 6a with $AlCl_3$ via its carbonyl group. Consequently, a shift of νC–F and νC–O modes of the methoxy and CF_3 groups of 6a is observed, while the band at 1164 cm^{-1} is related to νC–O–Al modes. Simultaneously, the intensity of the νC═C band is decreased. In principle, the same effects were observed when 6a interacts with $TiCl_4$ forming a bis-chelate complex.[32]

After admixture of 7, the most significant changes during the warming period from −60 °C to −1 °C resulted in the

Table 1. Frequencies (cm^{-1}) of Selected Bands Observed for 6a and Mixtures of 6a with Different Lewis Acids during Reaction in CH$_2$Cl$_2$

	ν(C=O)	ν(C−F)	ν(C−O)/ν(C−O−M)	
6a	1701/1684	1329	1193	1141
6a + TiCl$_4$	1636/1602	1339/1327/1313	1214/1202	1167/1147
6a + AlCl$_3$	1628	1350/1333	1214/1202	1167/1147

Figure 8. *In situ* UV−vis spectra recorded during the AlCl$_3$- and TiCl$_4$-mediated reaction using 0.5 mol L^{-1} and 5 × 10^{-4} mol L^{-1} of **6a/6b** in CH$_2$Cl$_2$: **6a/6b** at 20 °C, **6a** + AlCl$_3$ and **6b** + TiCl$_4$ at −60 °C in 1:1 molar mixture (the spectrum of TiCl$_4$ in CH$_2$Cl$_2$ is shown for comparison). Adapted with permission from ref 32. Copyright 2011 John Wiley & Sons, Inc. Adapted with permission from ref 49. Copyright 2013 Elsevier.

appearance of new bands at 1705 cm^{-1} (νC=O), 1615/1577/1521 cm^{-1} (νC=C), 1358/1323 cm^{-1} (νC−F), and 1194/1145 cm^{-1} (νC−O). These changes reflect the formation of an intermediate complex, which could not be assigned in detail. Nevertheless, the frequencies of the characteristic bands occurring during reaction indicated an analogous reaction pathway as observed in the TiCl$_4$-mediated reaction as can also be seen by comparing the respective spectra after reaction at −1 °C (Figure 7). However, analyzing the *in situ* spectra of mixtures containing **6a** and AlCl$_3$ as well as **6a** and TiCl$_4$ at −60 °C before admixture of **7** by means of typical band frequencies some differences, in particular for νC=O and νC−F vibrations, becomes evident (Table 1).

Comparing the respective UV−vis spectra obtained from **6a** and **6b** in CH$_2$Cl$_2$ and after admixture of AlCl$_3$ and TiCl$_4$, respectively, an opposite behavior relating to the observed band shifts is observable (Figure 8).

Because the reaction was carried out with, for appropriate UV−vis measurements, too high concentrations of **6**, the same experiments were also performed in diluted solutions. In this way the changes induced by interaction of the Lewis acid with **6** can be inspected more properly. Whereas in the case of AlCl$_3$, the absorption edge in concentrated solution and the absorption band in diluted solution are slightly blue-shifted, a redshift is observed in concentrated solution in the case of

TiCl$_4$. The spectra measured in diluted solution show a blue-shifted band at 252 nm as well as a red-shifted band at 320 nm which has been explained by the fact that TiCl$_4$ attacks the ketenacetale at two sites leading to an increased electron density in the C−O bond by electron delocalization so that this group becomes UV−vis active. This explanation is in accordance with the found bis-chelate complex structure.[32] The band shift observed in the diluted AlCl$_3$ containing solution is not significant. This was explained by the absence of dπ-electrons in the AlCl$_3$-complex which hinders the formation of metal-donor resonance structures. Otherwise, it could be possible that the interaction between AlCl$_3$ and **6a** is not strong enough to form a second chromophore as in the case of TiCl$_4$.

Summarizing the spectroscopic findings described above a specific interaction of **6a** with AlCl$_3$ could be detected; however, based on this no structure of the formed intermediate complex could be proposed. For this reason it was tried to crystallize this complex from a 1:1 mixture of the **6a** and AlCl$_3$ in CH$_2$Cl$_2$ by slow evaporation and cooling. Single crystals were isolated and their molecular structure was determined. The X-ray structure analysis revealed that an aluminum chelate complex **9** has been formed[49] which does not contain chloro ligands as found in the respective Ti complex **10** formed by interaction of **6** with TiCl$_4$ (Scheme 6).[32]

Scheme 6. Structures of the Aluminum Tris-Chelate Complex 9 Formed between AlCl₃ and 6a and the Bis-Chelate Complex Formed between TiCl₄ and 6a[a]
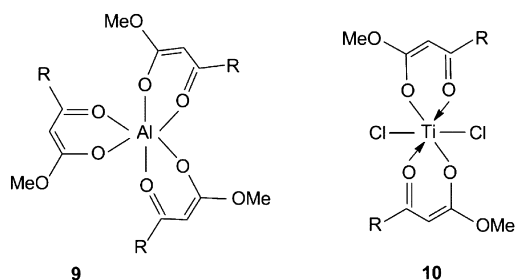
[a]According to the results of X-ray crystal structure analysis.[32,49] Reproduced with permission from ref 49. Copyright 2013 Elsevier.

Comparing the structures of both chelate complexes it can be expected that the aluminum tris-chelate complex **9** should be more stable than the chlorine-containing titanium bis-chelate complex **10**. Thus, the question arose if the isolated complex **9** is really an intermediate complex formed by reaction of AlCl₃ with **6a** in CH₂Cl₂. Inspecting the low frequency areas of the ATR-IR spectra of **6a**, the mixture of AlCl₃ + **6a** and **10** in CH₂Cl₂, significant differences are observable (Figure 9).
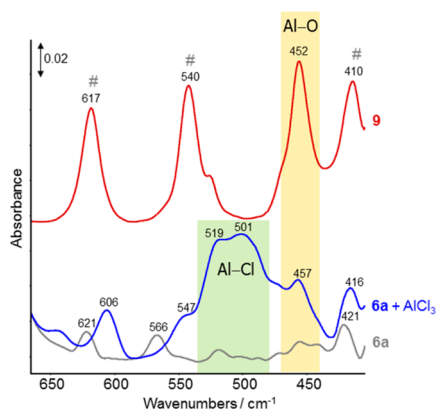

Figure 9. ATR-IR spectra of the crystallized Al-tris-chelate complex **9**, the reaction intermediate of **6a** + AlCl₃ and **6a** in CH₂Cl₂ ($c = 0.5$ mol L^{-1}) at 20 °C. The hash marked bands result from the butenone moiety (cf. Scheme 6). Reproduced with permission from ref 49. Copyright 2013 Elsevier.

The bands at 519/501 cm^{-1} observable only in the mixture of AlCl₃ + **6a** result from νAl−Cl modes which do not appear, as expected, in the spectrum of the aluminum tris-chelate complex **9**. Considering the hash marked bands of the butanone moiety of **9**, the band at 452 cm^{-1} can clearly be assigned to the νAl−O mode. The latter band and the bands of the butanone moiety appear slightly shifted in the spectrum of the intermediate formed complex of **6a** with AlCl₃. Thus, it was obvious that the intermediate complex formed *in situ* during the experiment has another composition and structure as the crystallized tris-chelate complex **9**. Considering that the latter complex **9** is formed by a longtime crystallization process, it is likely that the chlorine-containing aluminum complex is the first intermediate formed by interaction of AlCl₃ with **6a** which is then slowly transformed by losing chlorine. At the end, a stable chlorine-free aluminum tris-chelate complex is formed. According to literature data reported for an aluminum

trichloride-bidentate tertiary amine adduct **11** with trigonal bipyramidal coordination of the aluminum center,[50] a similar structure **12** was proposed for the observed intermediate complex formed between AlCl₃ and **6a** during the experiment (Scheme 7).

Scheme 7. Structure of the Aluminum Trichloride-Bidentate Tertiary Amine Adduct 11[50] and Postulated Structure of the Intermediate 12 Formed between AlCl₃ and 6a[a]
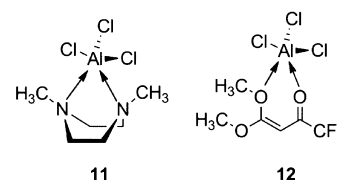
[a]Reproduced with permission from ref 49. Copyright 2013 Elsevier.

In conclusion, the *in situ* spectroscopic investigation of the Lewis acid-mediated cyclocondensation reaction between the ketenacetale **6** and the diene **7** showed that the AlCl₃-mediated reaction proceeds via a comparable mechanism as found for TiCl₄. Differences were observed in the mode of activation of the reactant **6** with AlCl₃. Real-time *in situ* spectroscopic investigation revealed the formation of an aluminum trichloride bidentate-butenone adduct as an intermediate while a crystallized chlorine-free aluminum tris-chelate complex was isolated from solution containing **6a** and AlCl₃ by long time crystallization at low temperatures. This might be perceived as a discrepancy; however, this finding nicely demonstrates the benefit of *in situ* spectroscopic studies enabling the real-time detection of intermediates formed in the respective reaction.

5. SETUP AND PRACTICAL ASPECTS

In homogeneous catalysis, there are often several restrictions concerning catalyst and reactant concentrations because the used substrates or ligands are partly expansive or merely low amounts are available. Therefore, normally a small volume of reaction solution is used. Taking into account that the reaction mixture has to be stirred, heated or cooled and kept under inert gas, a special design for an appropriate analytic reaction cell is required. Therefore, a versatile setup was developed[32−34] and employed for all *in situ* spectroscopic studies discussed above. Figure 10 shows a schematic of this setup and a picture of the realistic reaction cell allowing the simultaneous registration of ATR-IR, UV−vis, and Raman spectra using fiber-optic probes for each spectroscopy.

In this cell, 5−15 mL of solution can be properly handled, mixed by an external or magnetic stirrer, as well as heated or cooled by a heating plate/heating bath or cooling bath, respectively. To avoid evaporation of the solvent during heating, a cooling finger can by inserted and, if necessary, the reaction cell can be additionally flushed with inert gas.

Utilizing spectroscopic probes is generally straightforward for *in situ* spectroscopic studies of liquid and gas/liquid systems because of their flexibility and comparable easy handling. In multiphase systems, the monitoring of a solid catalyst by spectroscopic probes is usually not possible because of the very low attendant concentrations as, for example, in unsuccessful attempts using UV−vis reflection probes.[26] Nevertheless the problem can be solved for instance by integrating the ATR-IR technique into a special reactor design.[9,25,29]
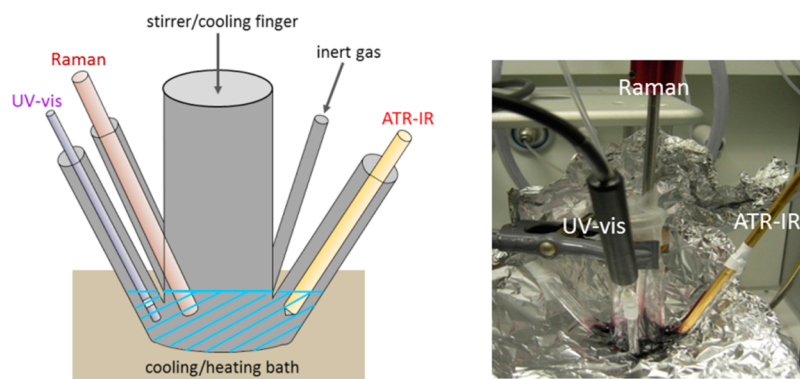
Figure 10. Schematic of the used setup (left) and the realistic analytic reaction cell (right) with implemented fiber optic probes for each spectroscopy.

Since quartz glass is transparent to Raman laser and UV–vis radiation, these spectroscopies are particularly versatile. Thus, the respective Raman laser optics can be focused also from outside, which is however accompanied by loss of sensitivity. In contrast, infrared radiation is strongly adsorbed by quartz; hence, special infrared transmissive fibers are required. Nowadays, silver halogenide fibers proven suitable are well established and used for the manufacturing of respective ATR-IR immersion probes which form part of the widely applied ReactIR system supplied by Mettler Toledo[12,16,17,51] or used in conjunction with conventional FTIR spectrometers[52–54] via respective coupled optics. It has to be noted that the ReactIR system is expensive and therefore not always the tool of choice, whereas standalone ATR probes linked with standard FTIR spectrometers offer a higher flexibility.

In the used setup (Figure 10), the UV–vis spectra were recorded with an AvaSpec 2048 fiber optical spectrometer equipped with an AvaLight-DHS light source and a special transmission probe with 1 mm gap (Avantes, Apeldoorn, The Netherlands). Raman spectra were recorded using a RXN1-785 Raman spectrometer equipped with a 10–400 mW diode laser for excitation at a wavelength of 785 nm and an Mk II Filtered Probe Head with an immersion optic (Kaiser Optical Systems). The measurements were performed with 70 mW. ATR-IR spectra were measured with a fiber optical diamond ATR probe (infrared fiber sensors, Aachen, Germany) which was connected to a Nicolet Avatar 370 FTIR spectrometer (Thermo Electron).

As can be seen from Figure 10, the used reaction cell has no special fittings so that the different experiments were restricted to perform at ambient pressure and temperatures from −70 to 100 °C which are, however, usual conditions for several types of homogeneously catalyzed reactions. Whereas the temperature stability of the probes is limited to ∼120 °C (UV–vis, ATR-IR) or 180 °C (Raman), the probes are pressure sealed up to 10 bar (UV–vis), 300 bar (ATR-IR), 200 bar (Raman), and therefore also applicable for reaction monitoring under higher pressures. For such investigations, the probes can also be implemented in special reaction cells or autoclaves[6,23,26] via Swagelok connections.

It has to be mentioned at this point that each spectroscopy requires a specific concentration level to get optimal information. Whereas complementary ATR-IR and Raman spectroscopy need rather higher catalyst and substrate concentrations, essential lower concentrations are necessary for UV–vis spectroscopy. Therefore, experiments using

different concentration levels are often needed to elucidate specific catalyst-substrate interaction as demonstrated in paragraphs 3 and 4. A further instructive example covering this aspect should be also mentioned at this place, the veratryl alcohol oxidation by Co(salen) in aqueous solution under oxygen.[27] On the basis of a detailed mechanistic study, the benefit of method coupling was nicely shown. Only by combination of UV–vis and ATR-IR spectroscopic studies carried out at different concentration levels, it was possible to identify three different Co(salen) complexes which are involved in the catalytic cycle: bis-μ-hydroxo[Co(salen)]$_2$ (ATR-IR and UV–vis), a Co(salen)-alkoxo species (ATR-IR), and a μ-peroxo-bridged alkoxy-Co(salen) species (UV–vis). The formation of the peroxo bridged species could not be observed by Raman spectroscopy which was obviously caused by its lower sensitivity (Raman spectra were recorded by focusing the laser beam on the glass reaction vessel externally).

Another possibility to overcome problems related to low catalyst concentrations, particularly in the case of IR spectroscopy, is to perform the measurements in transmission mode. Besides an essential higher sensitivity and good signal-to-noise ratio, this method enables access to metal–carbonyl vibrations which could not properly be detected by diamond ATR-IR probes because of overlapping diamond vibrations in the carbonyl frequency range. In particular, for *in situ* and *operando* studies of metal-catalyzed carbonylation reactions, which proceed normally under pressure, measurements in transmission mode are the tool of choice and are widely practiced using several sophisticated setups.[7,8,19,20] Despite the mentioned advantages of transmission measurements, the broad applicability and high flexibility of fiber optical ATR probes argue for their utilization in particular for the *in situ* monitoring of reactions in the liquid phase.

Looking at the discussed examples of use, it is obvious that coupling of ATR-IR, UV–vis, and Raman spectroscopy in one experiment makes no sense in either case. The selection of methods used is determined by the specific problems arising from the particular reaction. Therefore, before assembly of the most appropriate techniques, preliminary investigations of the catalyst, reactants, and suitable solvents are necessary, and the available spectral information has to be checked. In metal-catalyzed reactions it is often helpful to combine ATR-IR and Raman spectroscopy to cover a broad frequency range. In this manner, characteristic vibrations of functional groups (ATR-IR) as well as metal–nonmetal vibrations (Raman) can be observed with comparable sensitivity, which is indispensable to

study catalyst—reactant interactions. If the reaction progress cannot be monitored *in situ*, additional analytics is helpful to get information concerning the reactant conversion in the spectroscopic reactor. Only in this way the spectroscopic findings can be properly correlated with catalytic results, which is important to identify the really active species in the respective reaction.

For the sake of completeness, it should be mentioned that also kinetics can be well studied by combining *in situ* spectroscopic methods which was, however, not the aim of this paper. The determination of reactant conversion and product formation rates by analyzing band intensities in dependence on time gives additional useful information in terms of the influence of different reaction parameters, for example. Furthermore, *in situ* spectroscopy can be used for process control and, thus, optimizing the reaction conditions.

6. CONCLUSIONS

In situ spectroscopic methods like ATR-IR, Raman, UV—vis spectroscopy, and combinations of them proved to be powerful to get insight into catalyst action and the reaction mechanism in homogeneously catalyzed reactions. Because each spectroscopic method provides specific information, the suitable method combination has to be selected depending on the type of catalytic reaction and the particular questions. The discussed examples of use comprise only a narrow field of application possibilities. However, it was the primary aim of this work to show the variability of *in situ* spectroscopic methods regarding investigation of mechanistic aspects in homogeneously catalyzed reactions.

Thus, the different mode of catalyst action was demonstrated on two exemplary reactions in which imides and amides are selectively reduced by phenylsilanes. In one reaction the silane and in the other reaction the carbonyl group of the amide is activated by the respective catalyst. These insights can be utilized for selection and development of more effective catalysts in such reduction reactions.

The benefit of method coupling could nicely be demonstrated in the Fe-catalyzed formic acid decomposition. Thus, based on the specific information provided by each method, the catalytically active intermediate iron complex could be identified and the influence of chloride admixture on this complex formation could be elucidated. The coupling of *in situ* spectroscopy and product analysis (*operando* spectroscopy), in particular when gases were produced, has been proved to be beneficial to identify the genuine active state of the reaction system. Furthermore, it could be shown that the solvent is involved in complex formation and interacts with the reactant. Such specific reactant—solvent interaction often plays an essential role in homogeneously catalyzed reactions. Therefore, the *in situ* spectroscopic investigation of such interactions can help to understand the specific role of the solvent and to choose suitable solvents for the relevant reaction.

Using the example of a Lewis acid mediated cyclization reaction, it was shown that crystallized and structurally characterized potential intermediates are not ever the real intermediates existing in solution under reaction conditions. This finding nicely demonstrates the benefit of *in situ* spectroscopic studies enabling the real-time detection of intermediates.

A certain problem of combining different spectroscopies in one experiment is the covering of different concentration levels because complementary ATR-IR and Raman spectroscopy need rather higher catalyst and reactant concentrations while UV—vis spectroscopy requires essentially lower concentrations for getting proper and evaluable spectra. In this case, separate experiments are necessary to check if the reactions proceeding in concentrated and diluted reaction solutions are comparably.

In summary, *in situ* spectroscopy offers a great potential for the real-time monitoring of reactions in the liquid phase, for mechanistic studies, as well as process control and kinetics. The application of *in situ* spectroscopy enables a deeper understanding of catalyst action and reaction mechanism, which is a precondition for the development of tailored catalysts and optimized reaction conditions.

■ AUTHOR INFORMATION

Corresponding Author
*E-mail ursula.bentrup@catalysis.de.

Notes
The authors declare no competing financial interest.

■ REFERENCES

(1) Weckhuysen, B. M., Ed. *In Situ Spectroscopy of Catalysts*; American Scientific Publishers: Stevenson Ranch, CA, 2004.
(2) Weckhuysen, B. M. *Chem. Soc. Rev.* **2010**, *39*, 4541−5072.
(3) Brückner, A. *Catal. Today* **2010**, *155*, 155−330.
(4) Arean, C. O.; Weckhuysen, B. M.; Zecchina, A. *Phys. Chem. Chem. Phys.* **2012**, *14*, 2125−2127. See also the collection of articles on the theme of operando surface spectroscopy , *Phys. Chem. Chem. Phys.* **2012**, *14*, 2128−2245.
(5) Selent, D.; Heller, D. In *Catalysis*; Beller, M., Renken, A., van Santen, R. A., Eds.; Wiley-VCH: Weinheim, Germany, 2012; pp 465−492.
(6) Knöpke, L. R.; Bentrup, U. In *Heterogeneous Catalysts for Clean Technology − Spectroscopy, Design, and Monitoring*; Wilson, K., Lee, A. F., Eds.; Wiley-VCH: Weinheim, Germany, 2014; pp 39−63.
(7) Garland, M.; Li, C.; Guo, L. *ACS Catal.* **2012**, *2*, 2327−2334.
(8) Diebolt, O.; van Leeuwen, P. W. N. M.; Kamer, P. C. J. *ACS Catal.* **2012**, *2*, 2357−2370.
(9) Andanson, J.-M.; Baiker, A. *Chem. Soc. Rev.* **2010**, *39*, 4541−5072.
(10) Meemken, F.; Baiker, A.; Schenker, S.; Hungerbühler, K. *Chem.—Eur. J.* **2013**, *19*, 1−13.
(11) Meemken, F.; Maeda, N.; Hungerbühler, K.; Baiker, A. *Angew. Chem., Int. Ed.* **2012**, *51*, 8212−8216.
(12) Carter, C. F.; Lange, H.; Ley, St. V.; Baxendale, I. R.; Wittkamp, B.; Goode, J. G.; Gaunt, N. L. *Org. Process Res. Dev.* **2010**, *14*, 393−404.
(13) Garland, M.; Li, C. *Top. Catal.* **2009**, *52*, 1334−1341.
(14) Li, C.; Chen, L.; Widjaja, E.; Garland, M. *Catal. Today* **2010**, *155*, 261−265.
(15) Rueping, M.; Bootwicha, T.; Sugiono, E. *Beilstein J. Org. Chem.* **2012**, *8*, 300−307.
(16) Foley, D. A.; Doecke, Ch. W.; Buser, J. Y.; Merritt, J. M.; Murphy, L.; Kissane, M.; Collins, St. G.; Maguire, A. R.; Kaerner, A. *J. Org. Chem.* **2011**, *76*, 9630−9640.
(17) Quian, Z.; Baxendale, I. R.; Ley, S. V. *Chem.—Eur. J.* **2010**, *16*, 12342−12348.
(18) Torres, A.; Perez, N. M.; Overend, G.; Hodge, N.; Heaton, B. T.; Iggo, J. A.; Satherley, J.; Whyman, R.; Eastham, G. R.; Gobby, D. *ACS Catal.* **2012**, *2*, 2281−2289.
(19) Kubis, Ch.; Ludwig, R.; Sawall, M.; Neymeyr, K.; Börner, A.; Wiese, K.-D.; Hess, D.; Franke, R.; Selent, D. *ChemCatChem* **2010**, *2*, 287−295.
(20) Kubis, Ch.; Selent, D.; Sawall, M.; Ludwig, R.; Neymeyr, K.; Baumann, W.; Franke, R.; Börner, A. *Chem.—Eur. J.* **2012**, *18*, 8780−8794.
(21) Hollmann, D.; Grabow, K.; Jiao, H.; Kessler, M.; Spannenberg, A.; Beweries, T.; Bentrup, U.; Brückner, A. *Chem.—Eur. J.* **2013**, *19*, 13705−13713.

(22) Rabeah, J.; Bauer, M.; Baumann, W.; McConnell, A. E. C.; Gabrielli, W. F.; Webb, P. B.; Selent, D.; Brückner, A. *ACS Catal.* **2013**, *3*, 95−102.

(23) Walther, G.; Knöpke, L. R.; Rabeah, J.; Checinski, M. P.; Jiao, H.; Bentrup, U.; Brückner, A. *J. Catal.* **2013**, *297*, 44−55.

(24) Caravati, M.; Grunwaldt, J.-D.; Baiker, A. *Phys. Chem. Chem. Phys.* **2005**, *7*, 278−285.

(25) Bürgi, T. *J. Catal.* **2005**, *229*, 55−63.

(26) Knöpke, L. R.; Nemati, N.; Köckritz, A.; Brückner, A.; Bentrup, U. *ChemCatChem* **2010**, *2*, 273−280.

(27) Kervinen, K.; Korpi, H.; Mesu, J. G.; Soulimani, F.; Repo, T.; Rieger, B.; Leskela, M.; Weckhuysen, B. M. *Eur. J. Inorg. Chem.* **2005**, *13*, 2591−2599.

(28) Littler, B. J.; Looker, A. R.; Blythe, T. A. *Org. Process Res. Dev.* **2010**, *14*, 1512−1517.

(29) Richner, G.; van Bokhoven, J. A.; Neuhold, Y.-M.; Makosch, M.; Hungerbühler, K. *Phys. Chem. Chem. Phys.* **2011**, *13*, 12463−12471.

(30) (a) Tolstoy, P. M.; Koeppe, B.; Denisov, G. S.; Limbach, H.-H. *Angew. Chem., Int. Ed.* **2009**, *48*, 5745−5747. (b) *Angew. Chem.* **2009**, *121*, 5855−5858.

(31) (a) Hollmann, D.; Gärtner, F.; Ludwig, R.; Barsch, E.; Junge, H.; Blug, M.; Hoch, S.; Beller, M.; Brückner, A. *Angew. Chem., Int. Ed.* **2011**, *50*, 10246−10250. (b) Hollmann, D.; Gärtner, F.; Ludwig, R.; Barsch, E.; Junge, H.; Blug, M.; Hoch, S.; Beller, M.; Brückner, A. *Angew. Chem.* **2011**, *123*, 10429−10433.

(32) Knöpke, L. R.; Reimann, S.; Spannenberg, A.; Langer, P.; Brückner, A.; Bentrup, U. *ChemCatChem* **2011**, *3*, 1459−1468.

(33) Das, S.; Addis, D.; Knöpke, L. R.; Bentrup, U.; Junge, K.; Brückner, A.; Beller, M. *Angew. Chem., Int. Ed.* **2011**, *50*, 9180−9184.

(34) Li, Y.; Molina de La Torre, J. A.; Grabow, K.; Bentrup, U.; Junge, K.; Zhou, S.; Brückner, A.; Beller, M. *Angew. Chem., Int. Ed.* **2013**, *52*, 11577−11580.

(35) Chuit, C.; Corriu, R. J. P.; Reye, C.; Young, J. C. *Chem. Rev.* **1993**, *93*, 1371−1448.

(36) Cyrański, M. K.; Jezierska, A.; Klimentowska, P.; Panek, J. J.; Żukowska, G. Z.; Sporzyński, A. *J. Chem. Phys.* **2008**, *128*, 124512.

(37) Sakakura, A.; Ohkubo, T.; Yamashita, R.; Akakura, M. *Org. Lett.* **2011**, *13*, 892−895.

(38) Maki, T.; Ishihara, K.; Yamamoto, H. *Tetrahedron* **2007**, *63*, 8645−8657.

(39) Johnson, T. C.; Morris, D. J.; Wills, M. *Chem. Soc. Rev.* **2010**, *39*, 81−88.

(40) Haszeldine, R. S. *Science* **2009**, *325*, 1647−1652.

(41) Boddien, A.; Mellmann, D.; Gärtner, F.; Jackstell, R.; Junge, H.; Dyson, P. J.; Laurenczy, G.; Ludwig, R.; Beller, M. *Science* **2011**, *333*, 1733−1736.

(42) Mellmann, D.; Barsch, E.; Bauer, M.; Grabow, K.; Boddien, A.; Kammer, A.; Sponholz, P.; Bentrup, U.; Jackstell, R.; Junge, H.; Laurenzy, G.; Ludwig, R.; Beller, M. *Chem.—Eur. J.* **2014**, submitted.

(43) Nakamoto, K. *Infrared and Raman Spectra of Inorganic and Coordination Compounds*, Part B; John Wiley & Sons, Inc.: New York, 1997; pp 54−56.

(44) Mink, J.; Németh, Cs.; Hajba, L.; Sandström, M.; Goggin, P. L. *J. Mol. Struct.* **2003**, *661−662*, 141−151.

(45) Edwards, H. G. M.; Lewis, I. R.; Turner, P. H. *Inorg. Chim. Acta* **1994**, *216*, 191−199.

(46) Siewertsen, S.; Schlehahn, H.; Homborg, H. *Z. Anorg. Allg. Chem.* **1993**, *619*, 1064−1072.

(47) Nakamoto, K. *Infrared and Raman Spectra of Inorganic and Coordination Compounds*, Part B; John Wiley & Sons, Inc.: New York, 1997; pp 59−62.

(48) Gibson, D. H.; Ding, Y.; Miller, R. L.; Sleadd, B. A.; Mashuta, M. S.; Richardson, J. F. *Polyhedron* **1999**, *18*, 1189−1200.

(49) Reimann, S.; Knöpke, L. R.; Spannenberg, A.; Brückner, A.; Kühn, O.; Langer, P.; Bentrup, U. *Tetrahedron* **2013**, *69*, 3338−3347.

(50) Altwood, J. L.; Jones, C.; Raston, C. L.; Robinson, K. D. *Main Group Chem.* **1996**, *1*, 345−347.

(51) Burke, A.; Hebrault, D. *Metal Catalyzed Transformations*, White Paper, Mettler Toledo, www.mt.com/autochem.

(52) Küpper, L.; Heise, H. M.; Butvina, L. N. *J. Mol. Struct.* **2001**, *563−564*, 173−181.

(53) Bentrup, U.; Küpper, L.; Budde, U.; Lovis, K.; Jähnisch, K. *Chem. Eng. Technol.* **2006**, *29*, 1216−1220.

(54) Minnich, C. B.; Buskens, P.; Steffens, H. C.; Bäuerlein, P. S.; Butvina, L. N.; Küpper, L.; Leitner, W.; Liauw, M. A.; Greiner, L. *Org. Process Res. Dev.* **2007**, *11*, 94−97.